Analytical Methods

Accepted Manuscript

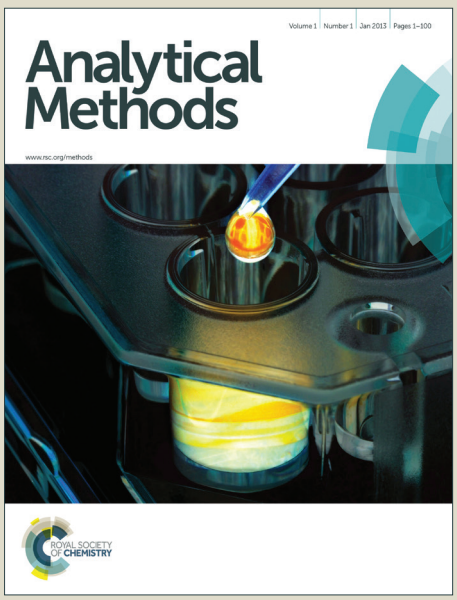

ROYAL SOCIETY OF CHEMISTRY

www.rsc.org/methods

Low-power micro-fabricated liquid flow-rate sensor

Wen-Chi Lin, Chemical Engineering, University of Michigan, Ann Arbo, Michigan 48197, USA
Mark A. burns, Chemical Engineering, University of Michigan, Ann Arbo, Michigan 48197, USA

***Abstract*—We have constructed micro-fabricated flow sensors that can measure water flow rates of 0.1 to 2.0 gallon per minute (GPM), and the experimental results we obtained are in good agreement with those from COMSOL simulations. Two identical sensors were fabricated on each device with an upstream sensor functioning as a temperature sensor, and the voltage difference between the two sensors indicating the water flow rate. The sensors were constructed on glass substrates, chosen for their low price, efficient thermal isolation, and compatibility with current water supply systems. The variation of water temperature of the flowing fluid from 10 to 50 ˚C was accounted for by normalizing the voltage readings. The dimensions of the sensors ranged from 71 µm by 80 µm to 430 µm by 480 µm with the smaller sensors having a higher sensitivity. Sensitivity also increased with increasing input power up to the point when boiling occurred. The optimized sensor, which was 71 µm by 80 µm on a 3 mm by 3 mm glass substrate, could be operated with only 2.75 mW of power in 10 to 50 ˚C water, providing an economic and energy efficient method to measure large water flow rates of 0.1-0.5 GPM.**

Keywords—flow-rate; thermal; micro-fabricated; sensor;

I. INTRODUCTION

Micro-fabricated thermal flow sensors have attracted considerable interest recently due to their small size, low power consumption, easy installation, and low per unit cost (less than a dollar if mass-produced). Thermal flow-rate sensors can be divided into three categories: time of flight, hot wire, and calorimetric [1].

Time of flight methods sense travel time for a heated bolus of fluid over a set distance [2]. These sensors are restricted in velocity measurements by data collection rates, and, in practice, their highest velocity detection is on the order of 10 cm/s. However, they have the advantage of directional detection of flow. Hot wire sensors detect the flow rate directly by changes in heater resistance. In most applications, these sensors cannot measure the direction of flow. Calorimetric sensors, ones that measure the temperature distribution around a heater, can detect the direction of the flow [3, 4].

Previous research in flow rate sensors has focused on calorimetric and hot wire methods measuring aerodynamic flow and small liquid flow at the level of μl/min or ml/min [1, 5, 6, 7, 8]. Shikada et al. have adapted micro-fabricated flow rate sensors for large-scale air flow, which is about 800 L/s [9, 10]. Others have developed a lower limit of a few nanoliters per minute [5], most of which are fluid temperature dependent. To compensate for the influence of fluid temperature, Ma *et al.* integrated a temperature sensor with the flow sensor [11], and the device worked successfully for air flow measurements. Koizumi et al. presented a fluid temperature-independent flow rate sensor, but it was only suitable over a small range (0.13-1.0 ml/min of water [1]).

Many of these sensors could have wide-spread use in applications such as municipal water supplies or chemical production facilities. However, flow rates on the order of gallons per minute (GPM) are common in these applications, and micro-fabricated flow sensors are rarely studied in this range. Aleksic et al. presented a flow sensor suitable for such flows, but the sensor was 25.4 mm by 6.35 mm and consumed 0.3-0.5 W of power [12]. Here we present a simple, cheap, small, and low-power sensor for high flow-rate liquid measurement. Using the micro thermal-capacitance technique, the sensor can measure water flow rates on the order of GPM in water temperatures of 10-50 ˚C translating to velocities of 10-250 cm/s. These flow rates and velocities in a one-inch-diameter pipe are common conditions in residential water supply systems.

II. FABRICATION AND METHODS

A. Simulation

The simulation was done with COMSOL version 4.3.0.184 operated on OSX version 10.9.2. The simulation was modified from the COMSOL non-isothermal flow package for turbulent flow. All material properties were imported form the COMSOL library. The Geometry was composed of 6mm wide and 2.9 mm tall water, and a 3 mm wide and 499 μm tall substrate on the top of which is a 3 mm wide, 1 μm thick film. The thin film was composed of five glass rectangles. Their lower boundaries were defined as boundary heat sources. The silicon and glass substrates were 499 μm thick. Fabricated film substrate was a combination of 1μm nitride and 498 μm thick air. Heat transfer of film and substrate was defined as heat transfer in solid. The left boundary of the water was defined as an inlet with constant temperature. Turbulent water from 0.062 m/s to 0.248 m/s velocity entered the region. The velocity was 0.5-2.0 GPM in a 1 in diameter pipe. The right boundary was defined as outlet with heat outflow, and upper and lower boundaries were defined as open boundaries.

In the simulation comapring the influence of substrates, the boundary heaters were 100 μm long and 2 mm apart from each other. Upstream and downstream sensors were provided with 5 W/m and 50 W/m power per length, which was equal to 0.5 mW and 5 mW for 100 μm wide sensors. Initial temperature was 30 °C. In the simulation comapring the influence of sensor size, the length of the heaters were 50 ,100, 200, 300 and 400 mm. In the influence of water-temperature test, the heaters were 50 mm long.

B. Sensor fabrication

RTDs made of Ti/Pt 300/1000 Å were deposited on glass wafer and protected by PECVD 1 μm glass film and 40 nm nitride film. Two identical heaters, 2 mm apart from each other, were aligned in the direction of flow on each probe. The upstream RTD worked as a temperature sensor and the downstream RTD worked as a flow rate sensor. The sensors were fabricated into the five different sizes shown in Table. The voltage on

each RTD was measured as output. Sensor resistances at different temperatures were measured with a multimeter to calculate the temperature coefficient of resistance (TCR), which should be 0.15 to 0.25 % and depends on the deposited thickness of platinum. The TCR of XS sensor was 0.24 %.

TABLE I. SENSOR SIZES

Size	**Longitude (μm)**	**Width (μm)**
XS	71	80
S	107.5	120
M	215	240
L	320	350
XL	430	480

C. Test setup

The schematic of the test setup was shown in Figure 1. Each probe was put into a one-inch-diameter pipe connected with a digital flow rate meter, a valve, and a circulating bath. Data was collected in different flow rate or flowing water temperature and repeated three times. The voltage difference of the two sensors was chosen to measure flow rate and avoid drift. The upstream temperature sensor was supplied with 0.5 mW.

The water temperature and input power of the downstream RTD varied in different testings. For heater size optimization, each probe was put in 30 °C flowing water and tested between 0.5-2.0 GPM. The upstream temperature sensor was supplied with constant 0.5 mW while the downstream flow rate sensor was supplied with 5 mW with constant DC current. For different water temperature tests, the XS probe was supplied 0.5 mW and 2.75 mW and exposed to 10, 20, 30, 40, and 50 ˚C water. Each experiment was repeated three times at each flow rate.

III. RESULT AND DISCUSSION

A. *Flow sensing using temperature*

General operation of the sensor

The temperature difference, ΔT, between the heater on the sensor and the flowing fluid is an indication of the liquid flow rate. As shown in Figure 2, when the heater is supplied with a constant power, P, this power is equal to the convective heat flux transferred to the flowing fluid, Q_f, plus the conductive heat flux transferred to the substrate, Q_s. The Nusselt number (i.e., the ratio of convective to conductive heat transfer) varies from 30 to 150 in this system, and, thus, the conductive heat flux transferred to the flowing fluid can be neglected. Q_f and Q_s can then be defined by Equations 1 and 2,

$$Q_f = hA_s\Delta T \quad (1)$$

$$Q_s = \frac{\Delta T}{R_s} \quad (2)$$

in which h is heat transfer coefficient, A_s is the heater size, and R_s is the substrate thermal resistance. ΔT is therefore defined by Equation 3:

$$\Delta T = \frac{P}{\frac{1}{R_s} + hA_s} \quad (3)$$

where R_s is defined as

$$R_s = \frac{L}{kA_c} \quad (4)$$

with k being the thermal conductive coefficient, L the distance to the edge of the substrate, and A_c the cross section area of the substrate.

A large value for R_s (i.e., small Q_s) is necessary for the sensor to function [7]. As shown in Figure 2 (a), when R_s is large, Q_f is much larger than Q_s, the first term of the denominator in Equation 3 is much smaller than the second term, and ΔT is dominated by convective heat transfer. Given that h is highly dependent on the liquid velocity, ΔT becomes a direct measure of the flow rate. Note that, as shown in Figure 2 (b), if R_s is small, which means Q_f is much smaller than Q_s, ΔT would be independent of the flow rate.

Conductive heat transfer to the substrate

The necessary high R_s value can be achieved through either material selection or microstructure fabrication. Material selection decreases k and microstructure fabrication decreases A_c, and they both increase R_s. For material selection, two common materials of 500 μm, the typical wafer thickness, were investigated and simulated: silicon and glass, with k values of 130 W/m·K and 1.38 W/m·K and thermal resistances of 3.5 K/W and 338 K/W, respectively. For microstructure fabrication, a thin film of 1 μm nitride was selected. With a k value of 18.5 W/m·K (not as insulating as glass), the R_s of the film is around 10^5 K/W with a small A_c.

As expected, the glass substrate performed much better than the silicon substrate. The influence of substrate materials is illustrated in a steady state 2D COMSOL simulation, as shown in Figure 3. Figure 3 (a) is the schematic of the simulated sensors. Figure 3 (b) illustrates the temperature distribution at 0.5GPM while Figure 3 (c) demonstrates the sensitivity, or the rate the temperature changes due to changes in the flow rate. In both Figure 3 (b) and (c), glass was preferable to silicon because it produced greater temperature changes. Further, silicon wafers need pre-deposition of an oxide film for electrical isolation. Using glass substrates improves device sensitivity and is also relatively inexpensive. The nitride thin film performed best, but production of this type of sensor is money- and time-intensive. Based on these results, their low price, and their compatibility with current water supply systems, we chose glass wafers for our experimental studies.

B. *Optimization of thermal flow rate sensor on glass*

Influence of the heater size

A smaller heater improves the device sensitivity and results in a higher ΔT in Equation 3. Figure 4 illustrates the correlation between the silmulated temperature on the sensor surface and A_s. Smaller sensors reached higher surface temperatures, resulting in a greater ΔT between the sensor and the flowing fluid. The temperature on the upstream temperature sensors changed 10 times smaller than the temperature on the downstream flow rate sensors. The temperature sensors that were 2000 μm away from the flow sensors were independent of water flow rate and, thus, could be used to measure water temperature.

The experimental results matched the simulations and indicated that smaller heaters improve device sensitivity for a given power input. The experimetal results using the XS probe are shown in Figure 5. As expected, higher flow rates produced lower voltage differences between the temperature sensor and the flow-rate sensor, thus allowing calculation of the flow rate. Figure 6 (a) illustrates the correlation between heater size and sensitivity using simulations, and Figure 6 (b) shows the experimental results. Although the 2D simulation is not an accurate representation of the experimental situation, both the simulation and experiments showed sensitivity decreasing with increasing sensor size. Sensitivity was defined by Equation 5, in which ΔV is the voltage difference change, V_{avg} is the average voltage difference, and ΔQ is the flow-rate change. Sensitivity of the simulation was calculated by translating simulated ΔT to ΔV with Equation 6, in which the temperature coefficient of resistance, α, was 0.2 % according to literature, the original resistance, $R_{0,}$ was 200 Ω, and the heater input power was 5 mW.

$$Sensitivity = \frac{\Delta V}{V_{avg}\Delta Q} \quad (5)$$

$$R = R_0(1+\alpha\Delta T) \quad (6)$$

Influence of the flowing water temperature

By using the water temperature sensor and the flow-rate sensor, the device can measure the water flow rate at different flowing water temperatures. Figure 7 (a) is the voltage readout of the temperature sensor on the device, which can be used to calculate the water temperature. Figure 7 (b) is the voltage difference between the voltage on the flow-rate sensor and the voltage on the temperature sensor. If the temperature sensor indicates the flowing water is 40 ˚C, the flow rate can be found by using the dash line and matching the voltage difference to the flow-rate line. Figure 7 (c) is the same data as in Figure 7 (b) plotted versus flow rate instead of temperature, and the curves show the relationship between voltage difference and flow rate at a given temperature. These curves can be collapsed into a single curve (Figure 7 (d)) by using a translated voltage difference, ΔV_m, defined by Equation 7. ΔV_{ref} is the readout at 2 GPM in the same water temperature.

$$\Delta V_m = \Delta V - \Delta V_{ref} \quad (7)$$

With the same sensor size, ΔT is higher in lower water temperatures, but ΔT can be normalized by theoretical or emperical translation. The ΔT of the COMSOL simulations for different water temperatues is shown in Figure 8 (a). To normalize the data, the functional form of h was derived from Equation 8.

$$Nu_{object} = 0.6\,\mathrm{Re}_p^{0.5}\mathrm{Pr}^{1/3} = \frac{hD}{k_w} \quad (8)$$

In Equation 8 Nu_{object} is the Nussult number around a non-spherical object, k_w is the thermal conductivity coefficient of water, D is the conduit diameter, Re_p the Renolds number around a particle, and Pr is the Prandtl number. Pr and the kinematic viscosity, ν, in Re_p change with the temperature of water, T, thus h is a function of T. The general form of that function can be derived from Equation 8 and is shown in Equation 9, in which B_1 is a constant.

$$h(T) = B_1 \nu^{-0.5} Pr^{1/3} \quad (9)$$

Thus, to define a temperture difference between the heater and the water, ΔT_{th}, which is indepent of T, Equation 3 can be modified into:

$$\Delta T = \frac{P}{\frac{1}{R_s}+hA_s} = \frac{\Delta T_{th}}{Bv^{-0.5}Pr^{1/3}} \quad (10)$$

The constant B in Equation 10 was set as 0.51 to let ΔT_{th} has the same average tempeture as ΔT. All curves in Figure 8 (a) can be normalized to Figure 8 (b) with Equation 11:

$$\Delta T_{th} = \Delta T(0.51v^{-0.5}Pr^{\frac{1}{3}}) \quad (11)$$

The curves in Figure 8 (a) can also be collapsed into a single curve (Figure 8 (c)) by using a emperically translated temperature difference, ΔT_m

$$\Delta T_m = \Delta T - \Delta T_{ref} \quad (12)$$

In which ΔT_{ref} is the ΔT that occurs at the highest flow rate (i.e., 2.0 GPM) in the same water temperature.

Figure 8 (a)-(c) shows that the sensor could measure 0.5-2.0 GPM in 10-50 ˚C water and that the influence of water temperature could be normalized. The sensor could also measure smaller flow rates, as shown in Figure 8 (d). The sensor could detect 0.1-2.0 GPM of water, and detection of smaller flow rates was also possible. The sensor was actually measuring velocities between 10 to 250 cm/s. This research focused on the application in 1inch diameter pipes, but using other pipe diameters, the sensor can be used for a wide range of flow rates and various applications. The 71 μm by 80 μm size also makes it possible to be used in micro-channels.

Influence of the input power

As the input power is decreased, the sensitivity of the device decreases. In Equation 3, ΔT is proportional to P, and increasing ΔT improves the sensitivity. In Figure 9, as research suggests [7, 11, 13], the sensitivity is propotional to the input power due to the higher temperature created at the sensor surface. Increasing the power too high, though, results in an inoperable sensor due to boiling. For the XS probe, increasing the input power over 20 mW caused the flow-rate sensors to become noisy and produce erratic results while the temperature sensors remained stable. The comparison of low and high input power signal was shown in

Figure 10. Figure 10 (a) was stable and supplied with 2.75 mW while Figure 10 (b) became noisy with 35.64 mW input power. Figure 11 shows the calculated temperature on the flow-rate heater using Equation 13, in which I is the input current, V is the voltage measured on the heater, and R_0 is the calculated resistance at zero input power. αR_0 was measured by a multimeter and was 0.275 for XS probes. The error bar was the temperature error calculated from input current and the standard deviation of the measured voltage. Sensor temperatures with more than 20 mW input power exceeded 100˚C, the boiling point of water under 1atm.

$$T = 30 + \frac{\frac{V}{I} - R_0}{\alpha R_0} \tag{13}$$

IV. Conclusion

This work presents a thermal flow-rate sensor that is integrated with a temperature sensor and can measure large flow rates up to 2 GPM (~0.1 L/s) in 10 to 50 ˚C water. Responding to velocity between 10 to 250cm/s, the sensor can also measure 0.2 to 7.8 mL/s water in 150μm wide micro-channels or 2 to 78 L/s water in 6inch diameter municipal pipes. Thus the sensor can span over 5 orders of magnitude in flow rates. And the sensors are fabricated with platinum, a metal that has not only the sufficient TCR for the flow-rate sensors to function but also the inert property to be used for other purposes such as water-sensing electrodes.

In terms of cost, the devices are 3 mm by 3 mm and can be fabricated with only one mask and a protection layer on the sensor surface. With this relatively simple fabrication, each device costs less than 30 cents, and more than 800 devices can be fabricated on a 4 in wafer. If fabricated on an industrial-sized 12 in wafer, around 7300 devices can be fabricated per wafer and the cost could be reduced even more. And note that adding electrochemical sensing using a platinum electrode on this device would not increase the cost since this metal is already present in the construction process—the construction of the extra sensors is essentially free.

ACKNOWLEDGEMENT

The authors thank the support from Brian N. Johnson, Klaus Brondum, and Leo Devota or their help and assistance in this work. This work was funded in part by a grant from the Masco Corporation.

REFERENCES

[1] H. Koizumi, "A micro flowmeter based on the measurement of a diffusion temperature rise of a locally heated thermal flow in a Hagen-Poiseuille flow," Flow Measurement and Instrumentation, vol. 34, pp. 19-26, 2013.

[2] H. Berthet, J. Jundt, J. Durivault, B. Mercier, and D. Angelescu, "Time-of-flight thermal flowrate sensor for lab-on-chip applications," Lab on a Chip, vol. 11, pp. 215-223, 2011.

[3] A. S. Cubukcu, D. F. R. Romero, and G. A. Urban, "A dynamic thermal flow sensor for simultaneous measurement of thermal conductivity and flow velocity of gases," Sensors and Actuators A: Physical, vol. 208, pp. 73-87, 2/1/ 2014.

[4] A. S. Cubukcu, E. Zernickel, U. Buerklin, and G. A. Urban, "A 2D thermal flow sensor with sub-mW power consumption," Sensors and Actuators A: Physical, vol. 163, pp. 449-456, 10// 2010.

[5] H. Ernst, A. Jachimowicz, and G. A. Urban, "High resolution flow characterization in Bio-MEMS," Sensors and Actuators, A: Physical, vol. 100, pp. 54-62, // 2002.

[6] T. H. Kim, D. K. Kim, and S. J. Kim, "Study of the sensitivity of a thermal flow sensor," International Journal of Heat and Mass Transfer, vol. 52, pp. 2140-2144, 2009.

[7] S. C. Roh, Y. M. Choi, and S. Y. Kim, "Sensitivity enhancement of a silicon micro-machined thermal flow sensor," Sensors and Actuators, A: Physical, vol. 128, pp. 1-6, 2006.

[8] B. Ma, J. Ren, J. Deng, and W. Yuan, "Flexible thermal sensor array on PI film substrate for underwater applications," Micro Electro Mechanical Systems (MEMS), 2010 IEEE 23rd International Conference, pp. 679-682, 2010

[9] M. Shikida, K. Yoshikawa, S. Iwai, and K. Sato, "Flexible flow sensor for large-scale air-conditioning network systems," Sensors and Actuators, A: Physical, vol. 188, pp. 2-8, 2012.

[10] M. a. Shikida, Yamazaki, Y.b, Yoshikawa, K.b, Sato, K.b "A MEMS flow sensor applied in a variable-air-volume unit in a building air-conditioning system," Sensors and Actuators, A: Physical, vol. 189, 2013.

[11] R. H. Ma, D. A. Wang, T. H. Hsueh, and C. Y. Lee, "A MEMS-based flow rate and flow direction sensing platform with integrated temperature compensation scheme," Sensors, vol. 9, pp. 5460-5476, 2009.

[12] O. S. Aleksic, M. V. Nikolic, M. D. Lukovic, S. O. Aleksic, and P. M. Nikolic, "Analysis and optimization of a thermal sensor system for measuring water flow," Sensors and Actuators A: Physical, vol. 201, pp. 371-376, 10/15/ 2013.

[13] D. N. Pagonis, G. Kaltsas, and A. G. Nassiopoulou, "Fabrication and testing of an integrated thermal flow sensor employing thermal isolation by a porous silicon membrane over an air cavity," Journal of Micromechanics and Microengineering, vol. 14, pp. 793-797, 2004

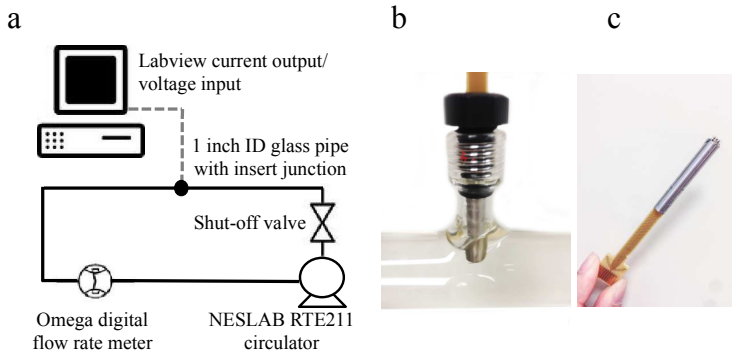

Fig. 1 – (a) The schematic of the experiment setup and the picture of (b) the glass tube insert junction and (c) the sensor probe.

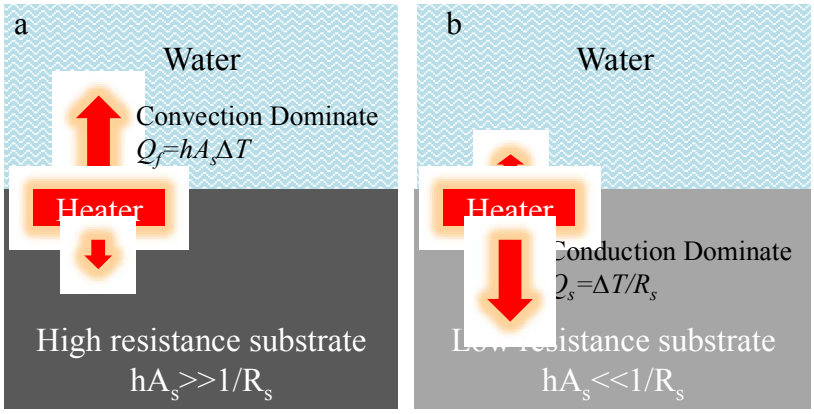

Fig. 2 – (a) Convection dominated and (b) Conduction dominated heat transfer.

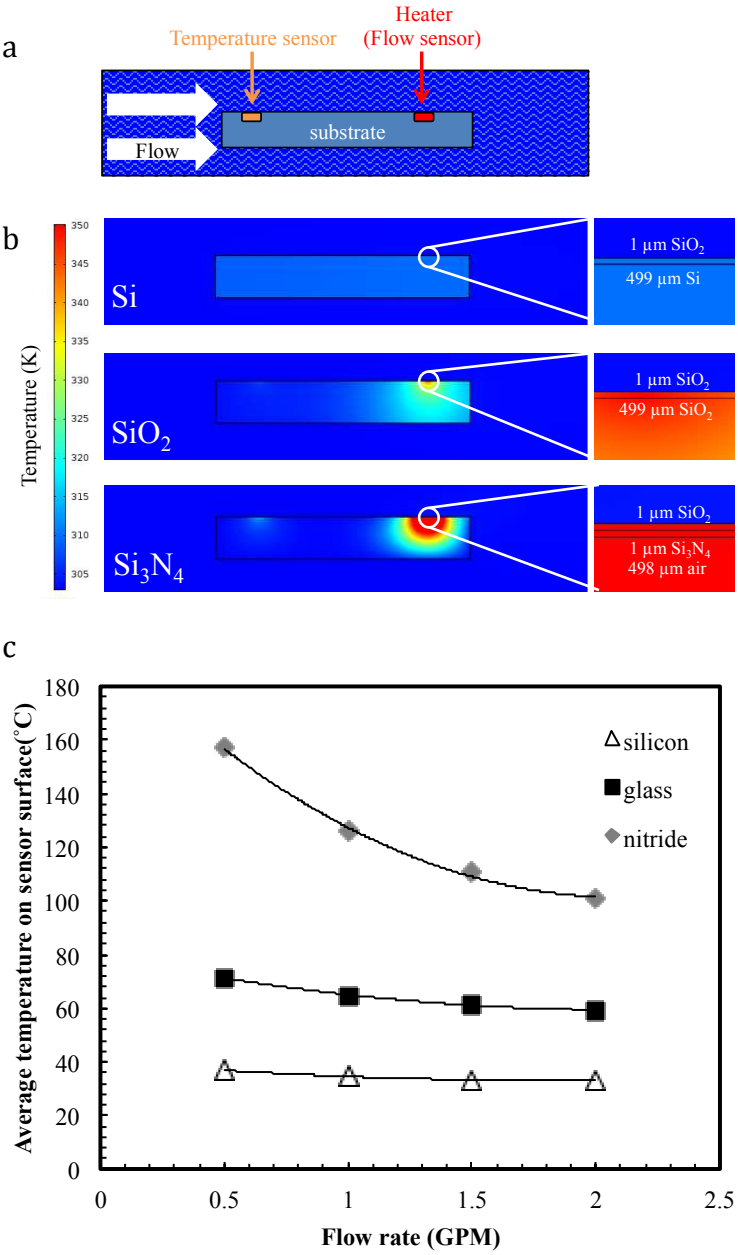

Fig. 3 – (a) The schematic of the sensor (b) The temperature field at 0.5GPM and (c) The correlation of heater temperature and flow rate of COMSOL simulation on different substrate.

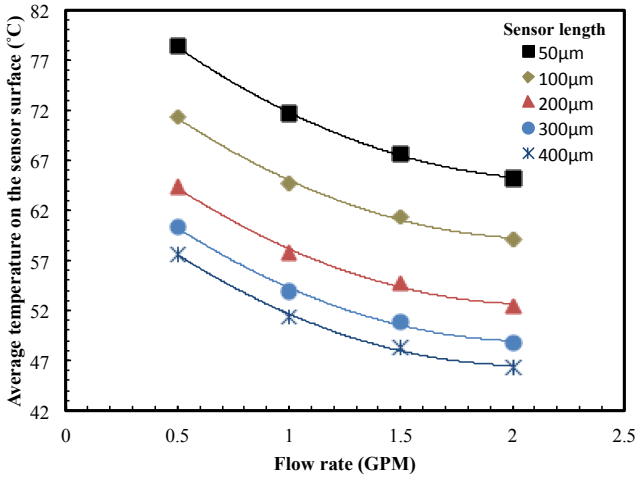

Fig. 4 – The temperature on the sensor surfaces in COMSOL simulation in various water flow rate. The heaters were supplied with 50W/m

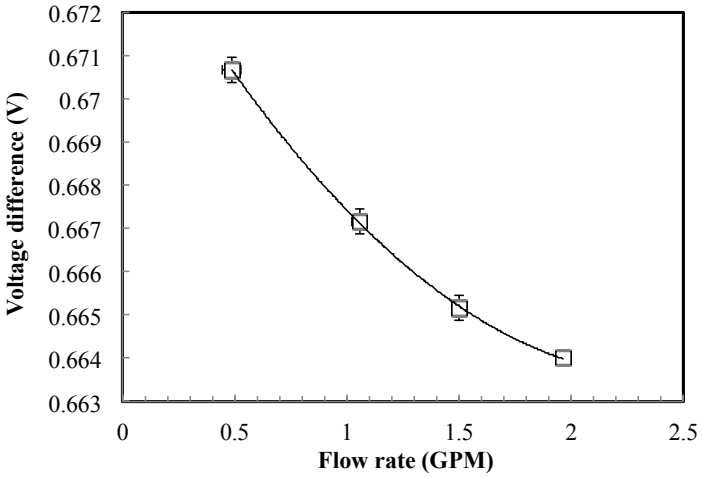

Fig. 5 – The experimental flow-rate sensing with XS sensor in 30°C water

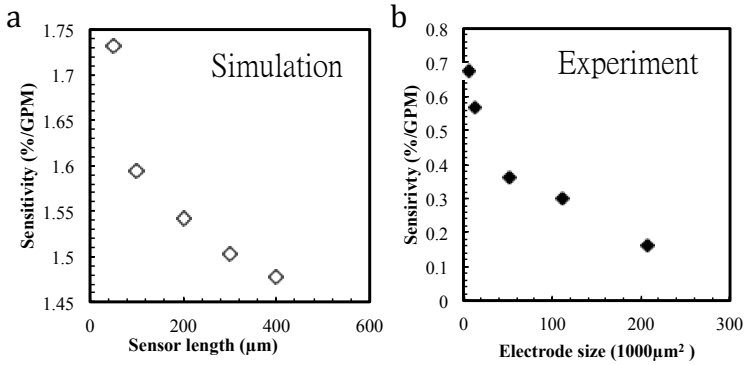

Fig. 6 – The sensitivity of (a) the simulation and (b) the experiment of various sensor sizes

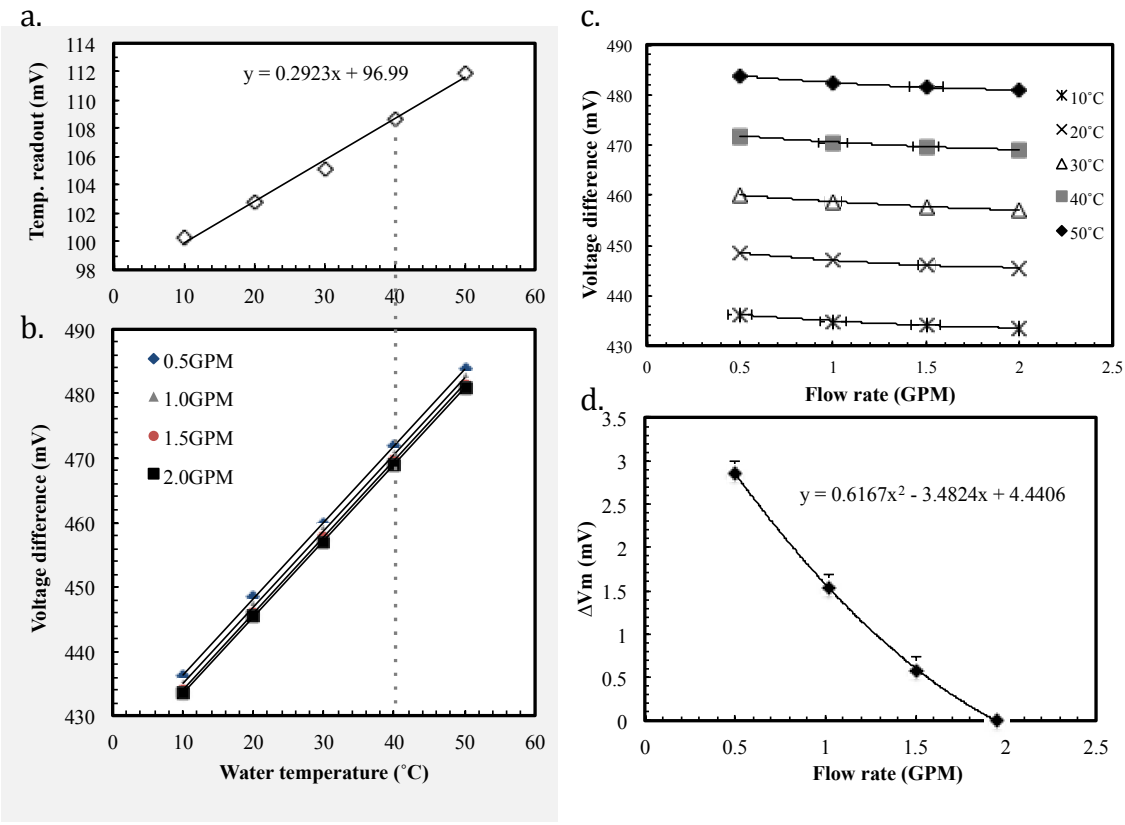

Fig. 7 – (a) The temperature sensor readout in mV versus the water temperature. The dash line is an illustration that 109mV temperature readout indicates 40°C of water, and the flow rate can be looked up by (b) the voltage difference or the flow-rate readout in different water temperature. (c) Voltage difference versus flow rate (d) Normalized curve ΔV_m defined by Equation 7.

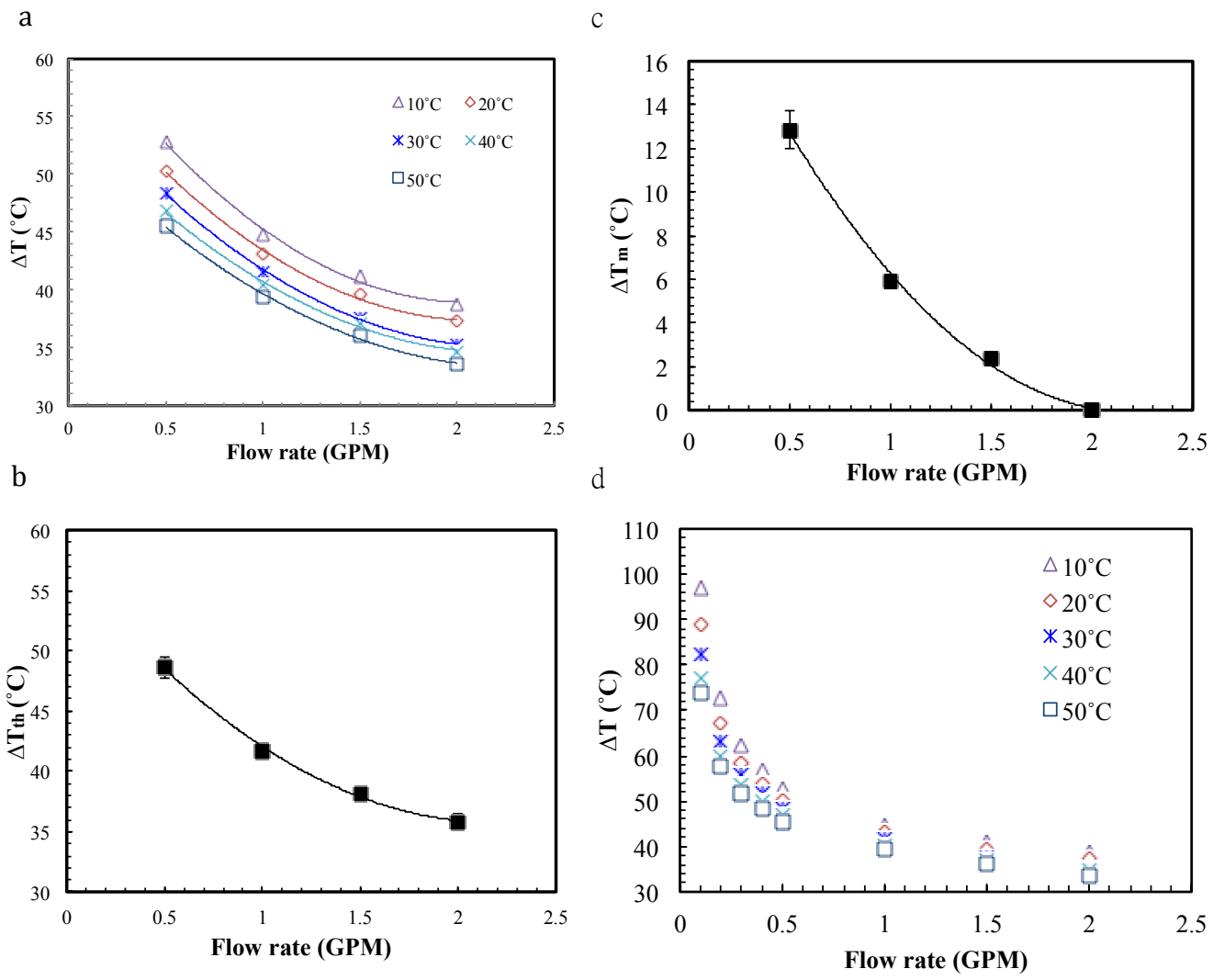

Fig. 8– COMSOL simulation in different water temperature of (a) ΔT and (b) ΔT_{th} (c) ΔT_m and (d) ΔT in 0.1-2.0 GPM.

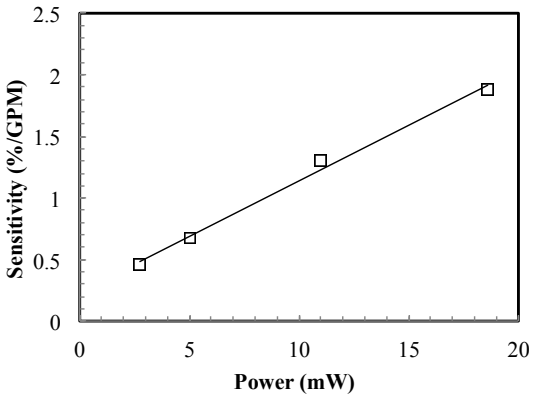

Fig. 9 – The input power and the sensitivity of XS sensor

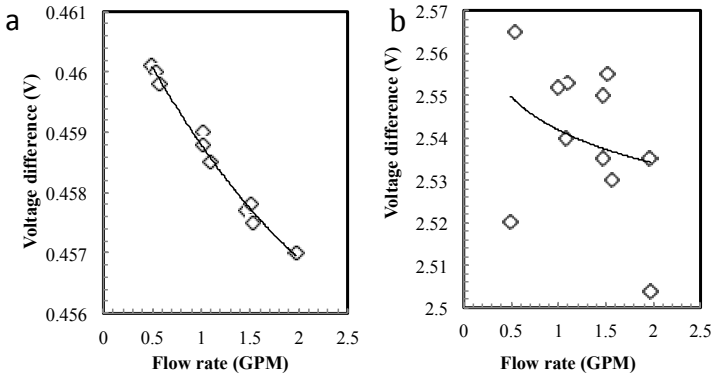

Fig. 10 – The raw data for the XS sensor supplied with (a) 2.75 and (b) 35.64 mW

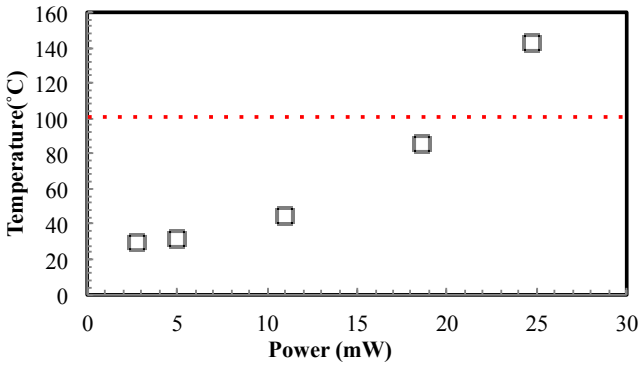

Fig. 11 –The calculated surface temperature of XS probes.